Selected Topics in Ultra-Low Emissivity Alpha-Particle Detection

Michael S. Gordon, *Senior Member, IEEE*, Kenneth P. Rodbell, *Senior Member, IEEE*, Henry H.K. Tang, *Member, IEEE*, Emmanuel Yashchin, *Member, IEEE*, Ethan W. Cascio, *Member, IEEE*, and Brendan D. McNally, *Member, IEEE*

***Abstract*—In an effort to better understand the contribution of terrestrial protons to the counter background, we have developed a model to examine the *production* of protons, within an ionization counter from the interaction of incident neutrons on the counter material. Results of high energy proton irradiation on an UltraLo-1800 XIA alpha-particle counter are shown which indicate that the active signal discrimination is very effective at rejecting most of the detected events. A Poisson model is described which gives guidance on making appropriate measurement times and acceptance criteria for detectors with a range of backgrounds.**

***Index Terms*—Alpha particles, ionization detectors, low-background, Poisson statistics, protons, terrestrial neutrons.**

I. Introduction

In PRIOR publications, the importance of reducing the alpha-particle component to Single-Event Upsets (SEUs) has been discussed [1]–[4]. The reduction in the alpha-particle component comes from using materials in the back-end-of-the line (wiring levels) and solder bumps with very low levels of Uranium and/or Thorium, reducing contamination of alpha-particle emitting elements, and shielding the alpha-particles where possible. It is now common that the alpha-particle emissivity of these materials is in the ultra-low category ($< 2\ \alpha/\mathrm{khr\text{-}cm^2}$). For reference, an alpha-particle emissivity of $2\ \alpha/\mathrm{khr\text{-}cm^2}$ corresponds to the detection of only $\sim 1.4\ \alpha/\mathrm{hr}$ on a 300 mm wafer. This emission rate is smaller than the typical background counting rate in conventional gas proportional counters. Recently ultra-low background ionization-mode counters from XIA have been shown to have backgrounds of around $0.3\ \alpha/\mathrm{khr\text{-}cm^2}$ [1]. This is due to the active signal rejection described in [1], [5]–[8] which is used effectively to reject alpha particles emanating from areas other than the sample. This relaxes the need for the use of ultra-low emissivity materials in the counter construction.

Manuscript received July 03, 2013; revised September 06, 2013; accepted October 14, 2013. Date of publication December 02, 2013; date of current version December 11, 2013.

M. S. Gordon, K.P. Rodbell, H.H.K. Tang, and E. Yashchin are with the IBM T.J. Watson Research Center, Yorktown Heights, NY 10598 USA (e-mail: gordonm@us.ibm.com).

E. W. Cascio is with The Francis H. Burr Proton Therapy Center at Massachusetts General Hospital, Boston, MA 02114 USA (e-mail: ecascio@partners.org).

B. D. McNally is with XIA LLC, Hayward, CA 94544 USA (e-mail: brendan@xia.com).

Color versions of one or more of the figures in this paper are available online at http://ieeexplore.ieee.org.

Digital Object Identifier 10.1109/TNS.2013.2287459

In [1] we showed that, using an XIA UltraLo-1800 alpha particle counter, the number of alpha particles detected from a 300 mm diameter silicon wafer sample increased by nearly a factor of 2 when the alpha particle detector was moved from a basement location to the top floor in the *same* building. We have recently observed similar behavior using a commercially available gas proportional detector in the same two locations.

Other classes of events besides the alpha particles from the same sample (mid air and round events) increased as well. We reported the results of a nuclear physics-based model which was used to estimate the number of alpha particles produced by neutron-induced reactions in the silicon sample and within the small active volume of gas above the sample. The model demonstrated that in the presence of terrestrial neutrons, a silicon substrate, with ostensibly zero alpha particle emission, would record an alpha particle emissivity of $\sim 0.3\ \alpha/\mathrm{khr\text{-}cm^2}$ in this ionization counter, at sea level in a room with no neutron attenuation. New alpha particle emissivity data [9] on the *same* 300 mm diameter silicon wafer sample, using the same brand of ultra-low background ionization counters has shown an identical neutron flux-dependence which supports, at least qualitatively, the results of the model.

Further, in [1], we discussed the origin of the signals induced on the anode of the XIA UltraLo-1800 alpha-particle counter including alpha particles from the sample, mid air, "round," ceiling and sidewall events. Mid air events were those events where the signal rise times were smaller than those expected from an alpha-particle emitted from the sample. These could arise from alpha particles emitted from radon gas originating in the counter materials. Round events refer to a class of events where the parabolic shape signal induced onto the anode, as the earliest electrons are collected, is too round compared to that predicted for its pulse amplitude (energy). These events occur from incident particles that have significantly smaller ionization in the Argon counter gas (dE/dx) than that of alpha particles. Ceiling events were those events with small rise times and small pulse amplitudes as one would expect from alpha particles emitted from the anode. Lastly, sidewall events are those which induce a signals on the guard electrode which is located at the same plane as, and outside of, the anode. If signals are induced on either the anode, or the guard electrode, both are recorded and the anode signal is fit for risetime, amplitude and rounding.

In this work, we examine four topics of interest in ultra-low emissivity alpha-particle detection. The first three of which help us understand the source(s) for the remaining, albeit extremely low, background in the UltraLo-1800 detector. First we describe a modeling effort where we consider the production of

protons from *within* the counter itself, and from the interaction of incident neutrons with the counter materials or sample substrate (Ar, plastic, and silicon). Second, we describe the energy loss of alpha particles and cosmic ray particles in the counter gas to understand their expected signature as they pass through the counter. Next, to demonstrate the effect of protons (either terrestrial, or produced from the neutron-induced protons) we exposed an XIA UltraLo-1800 alpha-particle counter to a beam of high-energy protons from the Francis H. Burr Proton Therapy Center at the Massachusetts General Hospital [10] and showed, as expected, the detector registers the presence of the high-energy protons. The active signal discrimination method, employed to suppress the counter background, is effective at rejecting most of the incident protons. Finally, given that we now have an ultra-low background detector for measuring the activity of our samples, we are interested in modeling the time required to ensure that our samples have alpha-particle emissivities lower than our specifications. This is a different problem than determining the time required to know the emissivity absolutely. To that end, we utilize the "Consumer-Producer" problem, common in statistical theory, as applied here to the issue of accepting a production lot of ultra-low emissivity raw material from a supplier. The model uses Poisson statistics and examines the confidence intervals for various measurement times so that the Consumer can have a certain level of assurance that the incoming material meets or exceeds the required specifications.

II. Proton Production via the (n,p) Reaction

We have modeled the interaction of terrestrial neutrons in the materials within the XIA UltraLo-1800 alpha-particle counter. The modeling setup follows the methodology which we used to calculate the alpha-particle flux generated from incident neutrons on silicon and in the argon gas [1]. In the current work, we were interested in proton production from the incident neutrons via (n,p) reactions. The calculations were Monte-Carlo simulations performed with IBM's SEMM-2 SEU system, [11] using nucleon-nucleon cross sections and nuclear reactions generated by the NUSPA code [12].

We used the energy differential flux of terrestrial cosmic neutrons at sea level [13] as an input to the calculations. The modeling considered the interaction of the normally incident neutrons with the ionization counter volume, consisting of plastic, the argon gas within the counter and a silicon substrate sample. Our simulation involves three transport problems: (1) the incident neutrons interacting with the plastic to produce secondary protons, (2) the incident neutrons passing through the plastic without nuclear collisions but interacting with the argon gas to produce secondary protons, and (3) the incident neutrons passing through both the plastic and the argon gas without nuclear reactions but interacting with the silicon to produce secondary protons.

In the first transport problem, the reactions of neutrons with carbon, oxygen and hydrogen are considered. For the cases of C and O, only inelastic scattering events are of interest (since elastic collisions would not produce protons) and the code selects those events that produce secondary protons, whereas in the case of H, elastic scattering events are the major source of the secondary protons. The calculation proceeds as follows. A collision point in the plastic region is selected. The reaction types ($\mathrm{n}+\mathrm{C}$, $\mathrm{n}+\mathrm{O}$, and $\mathrm{n}+\mathrm{H}$) is determined by a Monte Carlo procedure which takes into account the nuclear reaction cross sections of C, O and H and their densities in the plastic. From the positions, energies and velocities of the secondary protons, the code performs transport calculations to determine those protons which reach the interface between the plastic region and the Ar gas. The final energies of these protons which go into the Ar gas are computed.

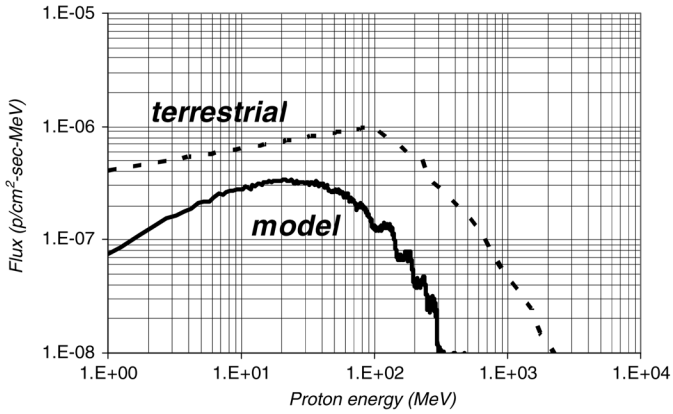

Fig. 1. Proton flux vs. incident proton energy for the simulation results of the (n,p) reaction described in this paper (solid line) and the published terrestrial proton flux from [15] (dashed line).

In the second transport problem, the reactions of $\mathrm{n}+\mathrm{Ar}\rightarrow \mathrm{p}+\mathrm{X}$ are analyzed, using the neutrons that transport through the plastic region without nuclear collisions. The code determines the energies of the secondary protons produced in the gas.

In the third transport problem the reactions of $\mathrm{n}+\mathrm{Si}\rightarrow \mathrm{p}+\mathrm{X}$ are analyzed, using the neutrons that transport through the plastic region and Ar gas without nuclear collisions. The code determines the secondary protons that transport upwards back into the Ar gas, and computes their energies.

It turns out that more than 99% of the secondary protons were produced by the interaction of neutrons within the plastic, which is used to contain the Ar gas in the ionization counter. This is to be expected, for two reasons. First, the plastic has high hydrogen content, and the n-p scattering is an effective way to produce protons. Second, the protons have long range, (from SRIM simulations [14], the range of protons in the 10-100 MeV energy range in plastic is $\sim$ 1-100 mm) and hence the plastic is in general not very effective at stopping them. The solid line in Fig. 1 shows a spectrum of the protons flux as a function of energy from the (n,p) reactions, calculated in the three transport problems as outlined above. The dashed line in Fig. 1 is the terrestrial proton spectrum from Ibe [15].

The peak flux in the terrestrial proton spectrum is about 3X larger than peak flux shown in the (n,p) model calculations. Further refinements to our model could include considering the effect of incident neutrons that impinge on the alpha particle counter at angles other than normal, [16] and would increase the path length of the neutrons in the counter materials thus increasing the calculated proton flux. In contrast, the terrestrial proton flux is not expected to be attenuated appreciably, by low

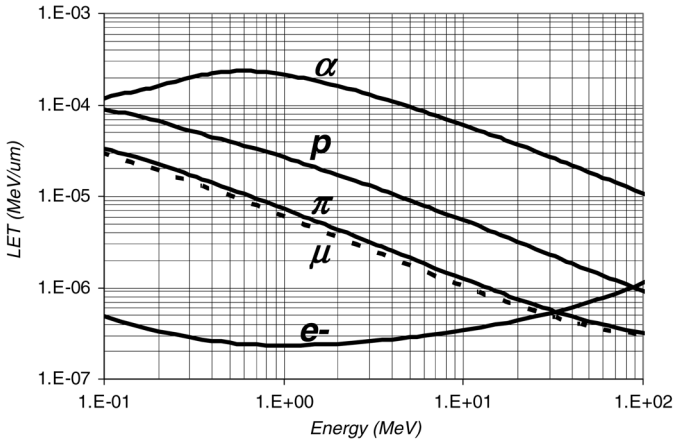

Fig. 2. The energy loss per path length for alpha particles, protons, pions, muons and electrons as a function of energy.

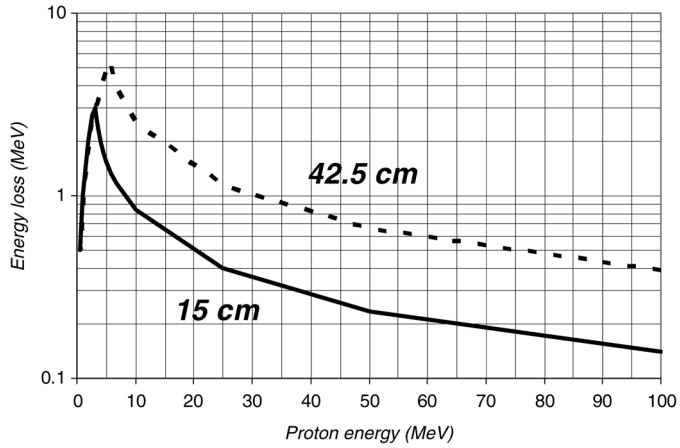

Fig. 3. The total energy loss for protons traversing 15 cm of argon (solid line) and 42.5 cm of argon (dashed line).

density building materials (e.g. concrete) above an alpha particle counter [17]. The effect of the terrestrial protons on the XIA UltraLo-1800 alpha-particle counter is on par with that from the neutron-induced (n,p) reactions of materials within the counter.

III. Energy Loss in Counter Gas

In order to further understand the interaction of cosmic ray particles in the UltraLo-1800 alpha particle counter, we evaluated the energy loss per path length in the argon counter gas using SRIM [14] for protons and alpha particles, SEMM2 [11] for pions and muons and [18] for electrons. These results are shown in Fig. 2. For incident energies above about 1 MeV, alpha particles have an energy loss of about 10X greater than that for protons of the same energy. Interestingly, both protons and alpha particles have similar energy loss in argon at ~ 0.1 MeV. Pions and muons have nearly identical energy loss in the argon counter gas, and both are about 5X lower than that for protons. Finally, electrons (or beta particles) have very low energy loss in the argon, except at very high energy.

For reference, the flux of muons at sea level is orders of magnitude larger than the proton flux at high energy, but on par at low incident energies [17], [19]. Since the energy loss per path length (Fig. 2) in argon gas is so much lower for muons compared to protons, and their flux is similar, at low energy, their contribution to signal formation in the alpha particle detector should be small, and only occur at the lowest of energies.

All alpha particles emanating from the sample are necessarily stopped in the counter gas, by design, since the anode to cathode spacing is larger than the alpha particle range in argon so the pulse height of the anode signal represents the energy of the alpha particles emitted from the sample. On the other hand, the energy loss per path length for particles with energies > 1 MeV is much smaller for the other particles of interest (protons, pions, muons and electrons), so their pulse height would simply represent their energy loss as they traverse (but don't stop in) the counter gas.

As an example of the range of energy deposited into the alpha particle detector by protons, we calculated the energy loss for protons with energy < 100 MeV in 15 cm and 42.5 cm of argon gas using TRIM [14]. The 15 cm and 42.5 cm distances correspond to the anode-cathode spacing and the length of the anode or cathode. The results are useful for determining the energy protons could deliver from vertically-oriented cosmic rays or from horizontally-incident (from an external source) proton beam. The results are shown in Fig. 3. The data shown by the solid line (dashed line) correspond to the energy loss in 15 cm (42.5 cm) of argon gas respectively. The peaks in the curves indicate the maximum incident energy where the protons are stopped in the gas.

Perhaps it is counter intuitive that the higher incident energy protons deposit less energy in the gas, since they do not stop in the gas, unlike the alpha particles emitted from samples. This example shows that the most energy that protons could deposit in the gas is a few MeV and occurs for the lowest incident proton energies.

IV. Proton Irradiation of XIA UltraLo-1800 Ionization Detector

An XIA UltraLo-1800 alpha-particle counter was transported to the Francis H. Burr Proton Therapy Center at the Massachusetts General Hospital and placed in two orientations (normal and tilted 25°) with respect to the external proton beam. Two experiments were carried out with the goal to see how many events of each class would be detected as a function of proton energy and flux.

As discussed in the introduction, and in more detail in [1], pulse shapes resulting from charge collection in the UltraLo-1800 have four distinct regions: the baseline of the signal which occurs before the ionization track is formed; a linear rise which occurs while all charges in the ion track are drifting towards the anode; a parabolic curve which starts when the first charges in the ion track are incident upon the anode, and ends when the last charges are collected from the track; and a decay region which occurs when charge collection has completed. The duration of the parabolic portion of the signal directly relates to the vertical projection of the charge track on the anode. Ionization tracks normal to the anode plane will be maximally parabolic, while ionization tracks parallel to the anode plane will have zero parabolic time.

The counter was tilted with respect to the external proton beam axis to increase the vertical projection of ionization tracks on the anode, and thus the likelihood of observing "round" events due to the passage of the protons incident upon the side of the detector.

In the normal operation of the ionization detector, terrestrial protons are generally incident from the vertical direction, whereas neutron induced protons can occur in any direction. Both of these protons sources will result in the detection of "round" events.

The initial 229 MeV proton beam from the cyclotron was degraded by using a combination of Pb or Pb and Lucite absorbers both to spread out and homogenize the beam and to lower the beam energy incident upon the front of the alpha-particle detector. The alpha particle detector was placed as far back from the degraders as possible. We estimate that the beam size was about 1 m^2 in area. We have shown through TRIM [14] simulations of protons incident upon the alpha particle detector, that $\sim$ 62 MeV is required to get through the outer detector housing (steel and aluminum), and plastic into the active detector volume. The energy spread of the proton beam (FWHM) increased due to the use of the degraders- with larger energy spread occurring at the lowest beam energy.

Tests were performed at incident (nominal) beam energies (at the front of the proton flux monitor) of 166.8, 102.7, and 69 MeV. The beam flux from the cyclotron had to be reduced by over 9 orders of magnitude from the nominal setup used for SEU exposures to ~ 0.03 p/cm^2-sec since the ionization detector was designed to operate at a trigger rate of few α/sec. In the first experiment, a 3" diameter X 3" thick NaI detector was used as a proton flux monitor since the conventional Faraday cup normally used for dosimetry could not record these low proton fluxes. This detector allowed us to lower the proton flux and perform preliminary experiments on the alpha particle detector with the external proton beam. Since the proton beam current is not completely stable at such a low flux, it was necessary to design a new large area flux monitor where the flux could be integrated.

In the second experiment, we used a large-area (9" X 14"), thick (0.8") plastic scintillator viewed edge-on by two 2" diameter photomultiplier tubes (PMT) as a proton flux monitor. The area of this plastic scintillator was roughly the same as the cross sectional area of the alpha-particle detector (anode-cathode spacing X anode width). The plastic scintillator was wrapped in an enhanced specular reflective foil[1], then in a light-tight plastic. The PMT's were coupled to the edge of the plastic scintillator with a silicone rubber pad.[2] The preamplified signals from the each PMT base were individually amplified then summed to increase the light collection efficiency. A pulse-height discriminator was used to separate the pulses induced by the incident protons from the cosmic ray background and the residual radiation in the proton experimental room. Finally the pulses whose amplitude exceeded the discriminator threshold were counted and used to normalize the events detected in the alpha particle detector.

[1]3M Vikuiti Enhanced Specular Reflector

[2]Eljen EJ560

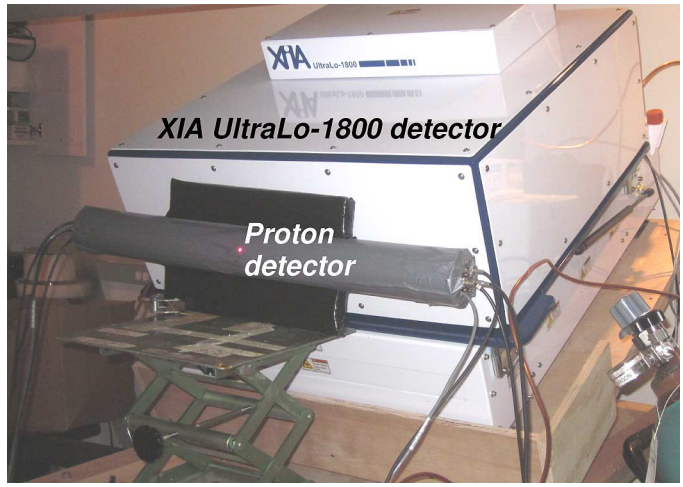

Fig. 4. Photograph of the XIA detector tilted 25° with respect to the proton beam. The plastic scintillator, used to measure the proton flux, is shown in front of the UltraLo-1800 alpha-particle detector. The red laser spot indicates the position of the proton beam.

Fig. 4 shows the Ultra-Lo 1800 ionization detector, in the tilted configuration as well as the proton flux monitor at the Francis H. Burr Proton Therapy Center at the Massachusetts General Hospital. The proton flux monitor was placed in front of the XIA Ultra-Lo 1800 alpha particle counter. The front panel of the alpha particle counter was temporarily removed and a laser used to align both proton flux detector and the height and position of the ionization portion of the alpha particle counter with respect to the proton beam. The laser spot is shown shining on the proton flux detector, in Fig. 4. Both PMTs were aligned with respect to the edge of the plastic scintillator with a cardboard tube as shown in the figure. We used ultra-high purity argon gas from a high-pressure cylinder, rather than the usual boil off from a liquid argon dewar.

Data for each run were recorded for 30 minutes, with the beam turned on after the first 5 minutes so that we could observe the transition in detected events. The number of proton events, detected by the proton flux monitor were simultaneously recorded and used to normalize the events detected by the alpha particle detector as discussed later. Runs were made with the counter tilted, as shown in Fig. 4, to accentuate the number of round events, as discussed earlier, and untilted. Additionally, we operated the counter in the "wafer" and "full" modes for both the tilted and untilted configurations at 169 MeV. In the "wafer" mode, the anode and cathode are 300 mm in diameter (707 cm^2), and in the "full" mode the anode and cathode are 42.5 cm X 42.5 cm (1800 cm^2). The guard electrode accommodates either mode- so that events inducing charge outside of the anode, onto the guard electrode, are summarily rejected (and labeled "sidewall").

Fig. 5 shows a representative scatter plot of the anode signal rise time plotted as a function of the pulse height for the 169 MeV run with the alpha particle detector tilted, in the "full" mode. The events registered by the detector were classified based on their risetime, pulse amplitude, and roundness, as discussed earlier. The black dots represent alpha particles, the blue dots represent mid air events, the purple dots represent

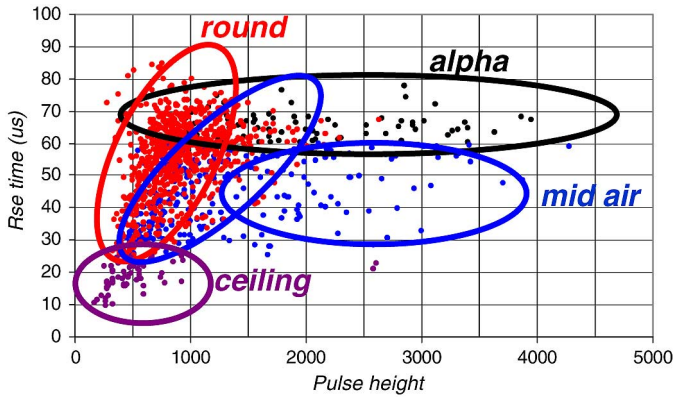

Fig. 5. Scatter plot of the anode signal rise time as a function of the anode pulse height for events detected in 30 minutes (25 minutes under proton irradiation) with the 169 MeV incident proton beam. The black dots represent alpha particles, the blue dots, the mid air events, the purple dots represent ceiling events, and the red dots, the round events.

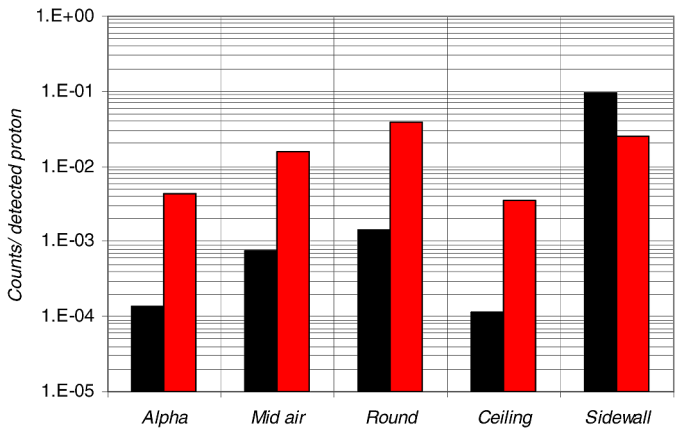

Fig. 6. Chart showing the number of alpha, mid air, round and sidewall events for the tilted configuration, in the "wafer" mode, shown in black, and the "full mode, shown in red, for an incident beam energy of 169 MeV. All data have been normalized to the proton flux.

ceiling events and the red dots represent the round events. For reference, a 30 min run was performed in the absence of protons, in the same detector configuration. One alpha, two mid air, zero round events and zero ceiling events were detected during that time period. Clearly the alpha particle detector registered a substantial number of proton-induced events, well in excess of the "background." Even though the alpha particle detector recorded the presence of the proton-induced events, the percentage of events identified as "alphas" compared to all events induced on the anode (alphas, mid air, ceiling and round) was a few percent.

Shown in Fig. 6 is a chart of the number of alpha particles, mid air, round, ceiling and sidewall events *per detected proton* for the detector in the tilted configuration, with 169 MeV incident protons. The data shown in black were taken in the "wafer" mode and the data shown in red were taken in the "full" mode. The data show more events of all types except the sidewall events for the "full" mode compared to the "wafer" mode. Both effects are to be expected since the anode area is larger, by 2.5X in the "full" mode compared to the "wafer" mode- whereas the

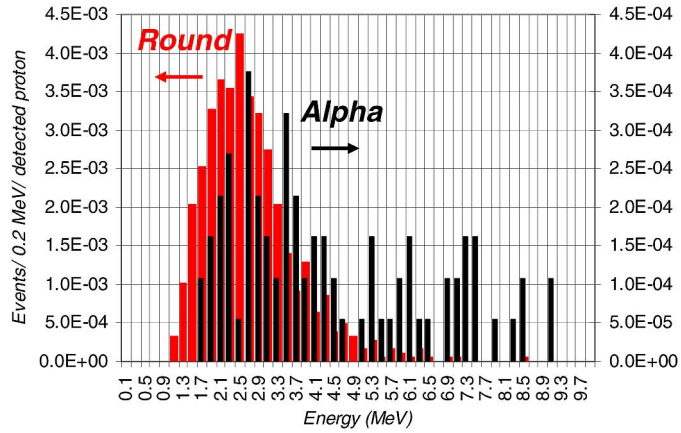

Fig. 7. Energy spectra for the alpha particles and round events for the tilted configuration, shown in black and red, respectively, for 169 MeV beam energy. All data have been normalized to the proton flux. The right hand scale goes with the alpha data- units are events/ 0.2 MeV/ detected proton.

guard electrode is similarly larger in the "wafer" mode compared to the "full" mode. What is surprising is that the ratio of the number of events in the "full" to "wafer" modes is significantly greater than the expected ratio of 2.5X.

Of the 81 alpha particles detected in the "full" configuration, shown in Fig. 6, about 1/3 had energies less than 3 MeV. The signal amplitude for low energy alpha particles is small, which adds to the uncertainty in the determination of the "roundness" and thus the determination as to whether these events are labeled as alpha particles or round events.

The energy of the alpha particles and round events for the "full" configuration depicted in Fig. 6 were binned into 0.2 MeV-wide bins, and normalized to the number of proton events, as described earlier. Histograms of these data are shown in Fig. 7- where the alpha particle data are shown in black (right hand scale) and the round events in red (left hand scale).

As expected from the discussion in Section III, the average energy in the round events is ~ 2.5 MeV since the protons can not deposit appreciable energy into the counter gas, independent of their incident energy. In contract, the energy of the alpha particles extends to ~ 9 MeV. Most likely these high energy events are truly alpha-particles generated from the (p, α) reaction in the argon gas as discussed in [1].

Lastly we show the normalized number of events of all types, for the tilted counter, in "full" mode, as a function of incident proton energy. The data shown in black, red and blue represent incident proton energies of 167, 102.7 and 69 MeV, respectively.

The most striking feature of the data shown in Fig. 8 is the large reduction of events of all classes at the lowest incident proton energy. This is most likely due to the energy loss of the incident protons through both the proton flux monitor, and then through the alpha particle detector housing. Using TRIM [14] we have determined that the energy loss of the protons with *nominal* energy of 69 MeV through the proton flux detector is ~ 25 MeV- which means that these protons do not have enough energy to penetrate the active alpha particle detection volume. On the other hand, there is a large spread in the beam energy, so that the few protons with larger energy than the nominal can get

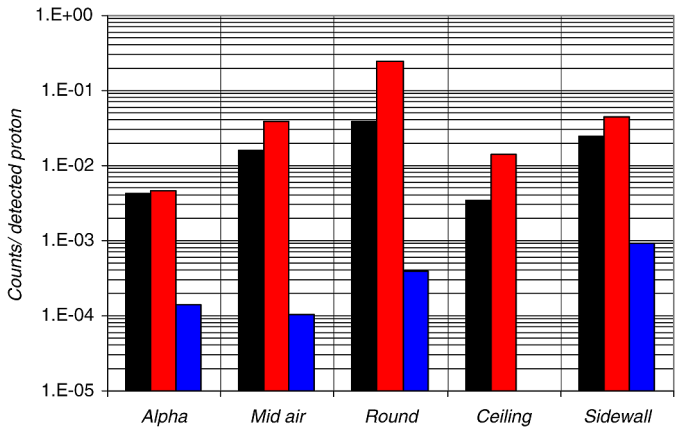

Fig. 8. Chart showing the number of alpha, mid air, round and sidewall events for the tilted configuration, in the "full" mode, for different incident proton energies: black: 167 MeV, red: 102.7 MeV, and blue: 69 MeV. Once again, all data have been normalized to the proton flux.

through both the proton flux detector and the alpha particle detector housing. The increase in the number of non-alpha particle events (mid air, round, ceiling, sidewall) at 102.7 vs 167 MeV is probably due to the increased ionization for the incident protons in the argon counter gas at the lower incident energy. Lastly, although the normalized number of alpha particles is nearly identical at the largest two proton energies, the number of high energy alpha particles is greatly reduced at 102.7 MeV compared to 167 MeV, as one might expect. The ratio of the number of alpha particles with energy > 5 MeV compared to all alpha particles detected, was 15% compared to 36% for the 102.7 MeV experiment, vs. the 167 MeV experiment, respectively.

V. Consumer-Producer Problem

With the ultra low background of the current generation of alpha particle detectors, it is now possible to make accurate measurements of ultra-low emissivity ($< 2\ \alpha/\mathrm{khr\text{-}cm^2}$) materials quickly [20]. Rather than determining what the ultimate emissivity of a sample is, we are interested in making a quick decision as to whether the alpha particle emissivity of the sample meets an emissivity specification.

This section describes a Poisson-based statistical model that can be used by the "Consumer," in order to ensure that materials provided by the supplier, or "Producer," meet the desired alpha-particle emissivity specification [21]. If a given lot of desired material is to be accepted, the Consumer conducts his own test of the alpha-particle emissivity. First, he measures the current background in his counter for time $\mathrm{T_b}$. Then he selects *at random* a single sample from the lot and measures the resulting combined (i.e., background plus sample) alpha-particle emissivity for time interval $\mathrm{T_s}$. Based on the difference of the alpha-particle emissivity observed during the intervals $\mathrm{T_s}$ and $\mathrm{T_b}$, the Consumer estimates the alpha-particle emissivity λ that is due to the sample. The objective of this test is to ensure, with a high level of confidence, that the alpha-particle emissivity λ of the sample does not exceed some pre-specified emissivity value, Λ. If the test leads to the conclusion that $\lambda < \Lambda$, then the sample, and the whole lot, is accepted; otherwise, the lot is rejected.

The Consumer also needs to provide some protection to the Producer, as excessive rejection of good lots will lead to high losses to the Producer (and higher costs for accepted lots). The Consumer specifies a given threshold level $\lambda_0 < \Lambda$ for which the probability of lot acceptance is reasonably high, say 90%. If the Producer manages to keep the emissivity of the sample below λ_0, he/she is rewarded with a high probability of product acceptance. In order to achieve the dual objective of protecting both himself and the Producer, the Consumer needs to make sure that both measurement times, $\mathrm{T_b}$ and $\mathrm{T_s}$, are sufficiently long. The Consumer also needs to use a statistically powerful model based on the expected sample and background count rates.

Of key importance is statistical modeling of the sample emissivity. It is one of the fundamental laws of physics that the process of emitting radioactive particles (like alpha-particles) follows Poisson statistics. In the following discussion, we use the following notation:

b–detector background
λ–alpha-particle emissivity of the sample
$\mathrm{T_b}$–length of time used to measure the detector background
$\mathrm{T_s}$–length of time used to measure the sample
Y–number of α-particles counted during the background measurement
X–number of α-particles counted during the sample measurement

In any alpha particle detector, the efficiency of detection is less than 1. Since the Poisson process of alpha-particle emission from a sample with emissivity λ and detected with a detector of efficiency p is still a Poisson process with intensity $\lambda \mathrm{p}$, all the methods in this paper are directly applicable to detectors of limited efficiency after re-scaling of the emissivity by p. Therefore, in what follows, we will assume, without loss of generality, that $\mathrm{p} = 1$.

In the following, we assume that the sample's area is 1000 $\mathrm{cm^2}$, so that the emissivity from the sample (in units of $\alpha/\mathrm{khr\text{-}cm^2}$) is equivalent to the alpha particle emission rate (in units of α/hr).

The model parameters are (b, λ); here b is a nuisance parameter. Since we are interested in the estimation of λ, of special interest are the confidence bounds for λ, as they can be used for quality assurance purposes.

Since the observables (X, Y) satisfy

$$\begin{aligned} X &\sim Poisson\{(b+\lambda) \times T_s\} \\ Y &\sim Poisson\{b \times T_b\} \end{aligned} \tag{1}$$

one could use the Likelihood methodology to carry out estimation. In particular, the log-likelihood $\ln(L)$, i.e., the logarithm of the probability of seeing the pair (X, Y) is:

$$\begin{aligned} \ln L(b, \lambda | X, Y) &= C + X \times \ln(b+\lambda) \\ &- (b+\lambda) \times T_s + Y \times \ln(b) - b \times T_b \end{aligned} \tag{2}$$

where C is a constant that depends on data only (i.e., it does not depend of the parameters b, λ). The Maximum Likelihood (MLE) estimates for ($b,\ \lambda$) are obtained by maximizing (2):

$$\hat{b} = Y/T_b$$
$$\hat{\lambda} = \max\{0, (X/T_s) - (Y/T_b)\} \tag{3}$$

Note that (3) are obtained by treating the likelihood function as a random variable in (X, Y), for any given ($b,\ \lambda$). When the test is complete, we will obtain the realizations $X = x, Y = y$, and by substituting (x, y) for (X, Y) in (3) we will obtain *estimates* for (b, λ) corresponding to a particular experiment.

Based on (2), we can also obtain the confidence bounds for λ by using the *profile likelihood* method [21]–[23]. In what follows, we will focus on the upper $(1-\alpha)\times(100\%)$ confidence bound for λ only and denote it by $\bar{\lambda}_{1-\alpha}$. To illustrate the use of this bound, let us assume that the Consumer receives a sample and needs to decide whether this sample's emissivity is acceptable. The testing can be implemented in terms of the following policy based on the alpha particle emissivity specification Λ and $\bar{\lambda}_{1-\alpha}$ (typically, $\alpha = 0.05$):

A. Consumer's Strategy

$$If\ \bar{\lambda}_{1-\alpha} > \Lambda\ then\ reject\ the\ sample$$
$$Otherwise,\ accept\ the\ sample \tag{4}$$

The motivation for this strategy is that the Consumer has an alpha particle specification Λ, and needs to be at least $(1-\alpha)\times(100\%)$ confident that this specification has not been violated. Clearly, if $\lambda = \Lambda$, then the probability of rejection is $(1-\alpha)$. In what follows, we will denote the rejection probability by $\mathrm{P_{reject}}$. We will also focus on the above strategy only; other possibilities are discussed in [21]. This strategy can also be implemented in terms of a simplified bound computation based on Gaussian approximation:

B. Gaussian Approximation

When the counts (X, Y) are large (~ 100), one could obtain confidence bounds of reasonable quality via normal approximation to distribution of $\hat{\lambda}$ given by (3). In particular, since

$$Var(\hat{\lambda}) \approx \frac{b+\lambda}{T_s} + \frac{b}{T_b} \approx \frac{X}{T_s^2} + \frac{Y}{T_b^2}, \tag{5}$$

the Gaussian approximation to the upper $(1-\alpha)\times(100\%)$ confidence bound can be obtained as follows:

$$\bar{\lambda}_{1-\alpha}(Gauss) = \hat{\lambda} + z_{1-\alpha}\sqrt{\frac{X}{T_s^2} + \frac{Y}{T_b^2}} \tag{6}$$

where $\hat{\lambda}$ is the estimate (3) and $z_{1-\alpha}$ is the $(1-\alpha)$–quantile of the Gaussian distribution (eg for $\alpha = 5\%$, $\mathrm{Z}_{1-\alpha} = 1.64$).

While the Gaussian approximation leads to confidence bounds that are "reasonable" when the counts (X, Y) are large, the current practice involves background levels as low as $\mathrm{b} = 0.3\ \alpha/\mathrm{khr\text{-}cm^2}$, and the sample alpha particle emissivity of interest is in the range of $\lambda < 2\ \alpha/\mathrm{khr\text{-}cm^2}$. Under such conditions, the Gaussian approximation becomes increasingly inaccurate, leading to distortion of risks that generally *works against the Consumer*. The reason for that is that consumer's protection is mostly governed by the upper confidence bounds for λ. Because the sampling distribution of $\hat{\lambda}$ is right-skewed, the Gaussian approximation produces upper bounds for λ that have less than nominal coverage, resulting in higher than anticipated risk of accepting substandard product [21].

In practice, however, the Consumer cannot act in a unilateral fashion based on strategy (4), because he needs to provide a certain level of protection for the Producer. Thus, the Consumer needs a good understanding of what levels of alpha particle emissivity λ can be considered acceptable. Accordingly, the consumer could pick an acceptable value λ_0 ($\lambda_0 < \Lambda$) and declare the following policy:

C. Consumer's Policy

(Step 1) Measure the background in an alpha particle counter for length $\mathrm{T_b}$. Denote by Y the number of alpha particles detected. The corresponding MLE of b is then $\hat{b} = Y/T_b$.

(Step 2) Calculate the necessary test time to measure the sample, $\mathrm{T_s}$ to satisfy:

$$P_{reject}(\lambda = \lambda_0 | Test\ Duration = T_s, b = \hat{b},) = \gamma, \tag{7}$$

where γ is a sufficiently small value that represents the *Producer's risk* (note that this equation can only be solved if $\mathrm{T_b}$ is sufficiently high).

(Step 3) Measure the alpha particle emissivity of the sample for length $\mathrm{T_s}$. Denote by X the observed number of alpha particles detected.

(Step 4) Compute the upper $(1-\alpha)\times(100\%)$ confidence bound $\bar{\lambda}_{1-\alpha}$(based on Y, $\mathrm{T_b}$, X, $\mathrm{T_s}$) and reject the sample if $\bar{\lambda}_{1-\alpha} > \Lambda$. Otherwise, accept the sample.

The above policy is implemented by selecting a sufficiently high $\mathrm{T_b}$ and using the Monte Carlo method (i.e., simulation) for solving (7). Typically, one can obtain a multitude of testing plans based on selecting various values of $\mathrm{T_b}$ above a certain threshold. One drawback of the above policy is that the total test time ($\mathrm{T_b} + \mathrm{T_s}$) cannot be known in advance, because the value $\mathrm{T_s}$ is established only after observing the background emissivity for time $\mathrm{T_b}$. In [21] some alternative policies are discussed. In what follows, we will focus on a particular policy that establishes ($\mathrm{T_b}, \mathrm{T_s}$) simultaneously by assuming that the background emissivity is known and equal to some "historically prevailing" value $\mathrm{b_0}$. The pair ($\mathrm{T_b}, \mathrm{T_s}$) is established by using the Consumer's Policy described above, with the only difference that for every selected $\mathrm{T_b}$, the corresponding value of $\mathrm{T_s}$ should satisfy the equation

$$P_{reject}(\lambda = \lambda_0 | Test\ Duration = T_s, b = b_0) = \gamma \tag{7a}$$

Unlike (7), the equation (7a) is not solved for every simulated case, but rather by a direct search: for every candidate value of

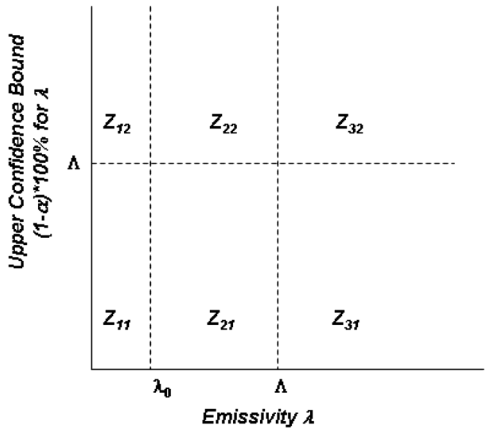

Fig. 9. The decision-making scheme related to the Consumer's strategy and policy described in sections A-C.

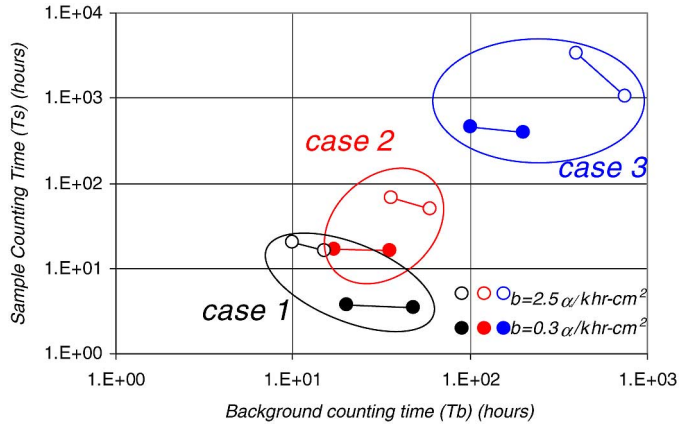

Fig. 10. Chart showing the sample counting time, $\mathrm{T_s}$ as a function of the background counting time, $\mathrm{T_b}$ for the three cases: case 1, $\lambda_0 = 0.25\ \alpha/\mathrm{khr\text{-}cm^2}$ (black), case 2, $\lambda_0 = 1.0\ \alpha/\mathrm{khr\text{-}cm^2}$ (red), and case 3, $\lambda_0 = 1.75\ \alpha/\mathrm{khr\text{-}cm^2}$ (blue). The closed circles correspond to $\mathrm{b} = 0.3\ \alpha/\mathrm{khr\text{-}cm^2}$ and the open circles correspond to $\mathrm{b} = 2.5\ \alpha/\mathrm{khr\text{-}cm^2}$.

$\mathrm{T_s}$ the sample counts are re-simulated, acceptance/rejection criterion is computed for every simulated case, and the difference between the LHS and RHS of (7a) is examined; this process continues until T_s is found for which the absolute value of this difference is smaller than some pre-specified small value ε. At this point we consider (7a) solved. Note that the resulting value $\mathrm{T_s}$ also solves the following problem: find the smallest value $\mathrm{T_s}$ for which the following inequality holds:

$$P_{reject}(\lambda = \lambda_0 | Test\ Duration = T_s, b = b_0) < \gamma \qquad (7b)$$

We also note that $\mathrm{b_0}$ is only used to help establish the testing times $(\mathrm{T_b}, \mathrm{T_s})$. The subsequent implementation of the policy is entirely data-driven. The value of $\gamma = 0.1$ is suitable for many practical applications. The examples shown in the following section represent pairs $(\mathrm{T_b}, \mathrm{T_s})$ satisfying (7a) and obtained via the simulation process described above. For every such pair $(\mathrm{T_b}, \mathrm{T_s})$ we compute the acceptance probability for various values of λ based on 50,000 simulated Poisson-distributed counts of particles.

In Fig. 9, we describe the decision-making scheme related to the Consumer's strategy and the policy described above. In this figure, the X axis corresponds to the sample emissivity λ and the Y axis gives the upper $(1-\alpha)\times(100\%)$ confidence bound for λ.

The plot is subdivided into six zones corresponding to the test outcomes:

$\mathrm{Z_{11}}$: The producer succeeded to maintain the sample emissivity below λ_0 and the sample was accepted by the consumer.

$\mathrm{Z_{12}}$: The producer succeeded to maintain the sample emissivity below λ_0 and the sample was rejected (the producer was punished undeservingly).

$\mathrm{Z_{21}}$: The producer did not succeed to maintain the sample emissivity below λ_0 but managed to stay within the specification Λ and the sample was accepted by the consumer.

$\mathrm{Z_{22}}$: The producer did not succeed to maintain the sample emissivity below λ_0 but managed to stay within the specification Λ and the sample was rejected by the consumer.

$\mathrm{Z_{31}}$: The producer did not succeed to stay within the specification Λ and got away with it.

$\mathrm{Z_{32}}$: The producer did not succeed to stay within the specification Λ and sample was rejected by the consumer.

D. Examples

In the following examples, we show the results of the model under two different background conditions, $\mathrm{b} = 0.3\,\alpha/\mathrm{khr\text{-}cm^2}$ and $\mathrm{b} = 2.5\ \alpha/\mathrm{khr\text{-}cm^2}$. In all cases, the Consumer wishes to have a rejection probability of 95% for the lot if $\lambda = \Lambda = 2\,\alpha/\mathrm{khr\text{-}cm^2}$ and the Consumer guarantees an acceptance probability of 90% for the following cases:

$$P_{accept}(\lambda = \lambda_0 = 0.25\ a/khr - cm^2 | b) \approx 90\%;$$
$$P_{accept}(\lambda = \Lambda = 2\ \alpha/khr - cm^2 | b) \approx 5\% \qquad \text{(case 1)}$$

$$P_{accept}(\lambda = \lambda_0 = 1.00a/khr - cm^2 | b) \approx 90\%;$$
$$P_{accept}(\lambda = \Lambda = 2\alpha/khr - cm^2 | b) \approx 5\% \qquad \text{(case 2)}$$

$$P_{accept}(\lambda = \lambda_0 = 1.75a/khr - cm^2 | b) \approx 90\%;$$
$$P_{accept}(\lambda = \Lambda = 2\alpha/khr - cm^2 | b) \approx 5\% \qquad \text{(case 3)}$$

The results are shown in Fig. 10, where the sample counting time, $\mathrm{T_s}$ is plotted as a function of the background counting time $\mathrm{T_b}$. The solid data points correspond to $\mathrm{b} = 0.3\alpha/\mathrm{khr\text{-}cm^2}$ and the open data points correspond to $\mathrm{b} = 2.5\ \alpha/\mathrm{khr\text{-}cm^2}$.

As the data in Fig. 10 shows, the test times needed to achieve the targeted acceptance properties are considerably shorter when the counter background is low (solid vs open circles). All three cases show that for both background conditions there can be more than one solution. All things being equal, one might chose, for example, the solution with the shorter sample measurement time, $\mathrm{T_s}$, or the one with the shorter total measurement time, $\mathrm{T_b} + \mathrm{T_s}$. Lastly, when $\lambda \ll \Lambda$ (case 1), the measurement time for the sample (and background) can be exceptionally short and still ensure that the sample's emissivity

is less than the alpha particle specification while still protecting the Consumer and Producer's interests. This is in contrast to the time required to determine the sample's true emissivity which is necessarily much longer. Note, however, that plans with very short total measurement time $T_b + T_s$ are not always advisable, see the Appendix.

VI. Conclusion

We have presented the initial results of our model showing that the terrestrial neutrons can produce a measureable proton flux within the structure of the XIA UltraLo-1800 alpha-particle counter. The overwhelming majority of these protons come from interactions of the neutrons with the plastic material which makes up the detection volume. The peak proton flux from these neutron-induced reactions on par with the terrestrial proton flux which shows that this reaction might contribute to the alpha particle counter's background.

As expected, modeling of the LET of terrestrial particles in argon counter gas showed that protons had about 10X lower LET compared to alpha particles and about 5X greater LET than either pions of muons. The LET for electrons (or beta particles) was several orders of magnitude lower than alpha particles. Additionally, we showed that the protons could only lose a few MeV at most in the counter gas. This implies that above ~ 3 MeV, there is probably very little contribution from cosmic ray particles.

Early results from a beam of high-energy protons shows that while the detector registers their presence, due to the active signal rejection, nearly all ($\sim 95\%$) of the protons are rejected and only a few are misidentified as alpha particles. As discussed, these might originate from (p, α) reactions in the counter. Presumably the model used to fit all of the signals that the detector records can be modified to reject an even larger fraction of events that appear to come from either terrestrial protons or neutron-induced protons particularly as more data become available.

Lastly we discussed a statistical model that we have developed which can be used to determine both background and sample measurement times, based on the expected background and sample counting rate given an emissivity specification. This model can be used to help in the decision of whether a specific lot of incoming material should be accepted or rejected based on statistics rather than qualitative factors. The analysis considered protecting the Consumer's interest, while rewarding the Producer who commits to high quality standards with high acceptance rates.

Appendix

In this Appendix we describe the performance (in terms of P_{accept}) of several plans and show that plans with minimal total test time ($T_b + T_s$) are not always advisable. Let us consider the case $\Lambda = 2\alpha$/khr-cm^2, $\lambda_0 = 0.25\alpha$/khr-cm^2, $b = 0.3\alpha$/khr-cm^2. Operating characteristics of several plans are shown in Table A.I and are plotted in Fig. A.1. Of special interest is the plan that corresponds to minimal total test time and in this case the plan ($T_b = 0.1$ hrs, $T_s = 4.4$ hrs) appears suitable: it protects both the Producer and Consumer, and the total test time is $4.5\text{hrs} = 0.1$ hrs $+ 4.4$ hrs is quite short compared to other plans considered in the table, namely, ($T_b = 20$ hrs, $T_s = 3.7$ hrs) and ($T_b = 48$ hrs, $T_s = 3.5$ hrs). Let us refer to these plans as P1, P2 and P3, respectively. As can be seen from Table A.I and Fig. A.1, these three plans not only guarantee the nominal Consumer and Producer protection, but also have comparable P_{accept} curves. The plans P2 and P3 are illustrated in Fig. 10 (Case 1). The good performance of the plan P1 relies heavily on the fact that the probability of observing one or more alpha particles in the very short period of time $T_b = 0.1$ hrs is only $1 - \exp(-0.3 * 0.1) \approx 3\%$, i.e., in most cases one will observe zero alpha particles during the background measurement period, leading to under-estimation of the background emissivity with probability $100 - 3 = 97\%$. With this in mind, one will need only $T_s = 4.4$ hrs to "resolve"

TABLE A.I
Acceptance Probabilities for Three Plans (T_b, T_s) Corresponding to the Case $b = 0.3\alpha$/khr-cm^2. The Threshold Value is $\Lambda = 2\alpha$/khr-cm^2, and the Acceptable Value is $\lambda_0 = 0.25\alpha$/khr-cm^2. The Last Column Corresponds to Acceptance Probability of the Test ($T_b = 0.1$ hrs, $T_s = 4.4$ hrs) Conditional on the Number of Observed Particles During Background Test Time $T_b = 0.1$ hrs Equal to $Y = 1$.

λ (α/khr-cm^2)	T_b = 0.1hrs T_s = 4.4hrs **Plan P1**	T_b = 20hrs T_s = 3.7hrs **Plan P2**	T_b = 48hrs T_s = 3.5hrs **Plan P3**	T_b = 0.1hrs T_s = 4.4 hrs, Y=1 **Plan P1***
0.1	96.5	96.2	95.5	100
0.25	90.1	89.9	88.5	100
0.5	72.7	75.2	72.0	100
1.0	35.3	39.2	36.9	99.3
1.5	13.2	15.8	15.0	94.1
2.0	5.16	5.43	5.36	77.5
2.5	2.10	1.79	1.74	54.5
3.0	0.86	0.63	0.51	31.4

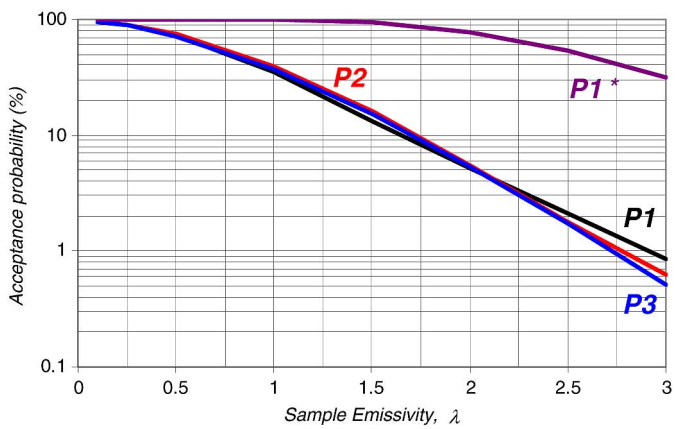

Fig. A.1. The acceptance probability curves (P_{accept}) as a function of the sample emissivity λ for the plans described in Table A.I

between $\lambda_0 = 0.25\alpha$/khr-cm^2 and $\lambda_0 = \Lambda = 2\alpha$/khr-cm^2. However, what happens if one actually observes an alpha particle within $\mathrm{T_b} = 0.1$ hrs? To analyze such a case, we perform a simulation study of the plan P1 conditional on $\mathrm{Y} = 1$. The results, plan $\mathrm{P1}^*$, are shown in the last column of Table A.I. One can see that the Consumer will end up accepting lots with emissivity levels as high as $\lambda = 3\alpha$/khr-cm^2 with probability 31.4%. This is the result of gross over-estimation of the background radiation in this case: in fact, its estimate is $1/0.1 = 10\alpha$/khr-cm^2. With such a high estimate of b, even the excess radiation as high as $\lambda = 3\alpha$/khr-cm^2 is not reliably detectable within $\mathrm{T_s} = 4.4$ hours. Plans P2 and P3 are much less risky in this respect–however, this comes at the expense of investing a much longer time in measuring the background. So, practical considerations will lead one to adopt a plan with relatively high $\mathrm{T_s}$, such as P2 or P3. Note that the plan with $\mathrm{T_b} = \infty$ effectively assumes that the background radiation is known and equal to $\mathrm{b} = 0.3\alpha$/khr-cm^2. Under such assumption, one could reduce $\mathrm{T_s}$ to 3.4 hrs–however, plans with a very high $\mathrm{T_b}$ are clearly impractical, except under special circumstances [21].

ACKNOWLEDGMENT

The authors would like to thank Dr. James Ryan and Jason Legere as well as Dr. Bernard Gottschalk for several discussions about plastic scintillators and efficient light collection, as well as loaning us several PMT's for this work.

REFERENCES

[1] M. S. Gordon, K. P. Rodbell, H. H. K. Tang, P. Ronsheim, Z. Zhu, S. Rauch, B. D. McNally, and S. Coleman, "Ultra-Low emissivity alpha-particle detection," *IEEE Trans. Nucl. Sci.*, vol. 59, no. 6, pp. 3101–3109, Dec. 2012.

[2] J. L. Autran, P. Roche, S. Sauze, G. Gasiot, D. Munteanu, P. Loaiza, M. Zampaolo, and J. Borel, "Altitide and underground read-time SER characterization of CMOS 65 nm SRAM," *IEEE Trans. Nucl. Sci.*, vol. 56, no. 4, pp. 2258–2266, Aug. 2009.

[3] J. L. Autran, D. Munteanu, P. Roche, G. Gasiot, S. Martinie, S. Uznanski, S. Sauze, S. Semikh, E. Yakushev, S. Rozov, P. Loaiza, F. Warot, and M. Zampaolo, "Soft-Errors induced by terrestrial neutrons and natural alpha-particle emitters in advanced memory circuits at ground level," *Microcircuits Reliab.*, vol. 50, pp. 1822–1831, 2010.

[4] J. L. Autran, S. Serre, D. Munteanu, S. Martinie, S. Semikh, S. Sauze, S. Uznanski, G. Gasiot, and P. Roche, "Real-Time soft-error testing of 40 nm SRAMs," in *Proc. IEEE Int. Reliability Physics Symp.*, 2012, pp. 3C.5.1–3C.5.9.

[5] W. K. Warburton, J. Wahl, and M. Momayezi, "Ultra-low background gas-filled alpha counter," U.S. Patent 6 732 059, May 4, 2004.

[6] W. K. Warburton and B. Dwyer-McNally, "Electronic background rejection in a new ultra-low background alpha particle counter," *Nucl. Instrum. Methods Phys. Res. B*, vol. 263, no. 1, pp. 221–224, Oct. 2007.

[7] W. K. Warburton, B. Dwyer-McNally, M. Momayezi, and J. E. Wahl, "Ultra-low background alpha particle counter using pulse shape analysis," in *Proc.IEEE Nuclear Science Symp. Conf. Rec.*, 2004, vol. 1, pp. 577–581.

[8] M. S. Gordon, D. F. Heidel, K. P. Rodbell, B. Dwyer-McNally, and W. K. Warburton, "An evaluation of an ultralow background alpha particle detector," *IEEE Trans. Nucl. Sci.*, vol. 56, no. 6, pp. 3381–3386, Dec. 2009.

[9] B. D. McNally, W. K. Warburton, and S. Coleman, "Preliminary results from a field assessment of the Ultra-Lo 1800," in *Proc. IEEE Santa Clara Valley Soft Error Rate Workshop*, San Jose, CA, USA, Oct. 25, 2012 [Online]. Available: https://sites.google.com/site/ieeescvserworkshop/Presentations.

[10] E. W. Cascio, J. M. Sisterson, J. B. Flanz, and M. S. Wagner, "The proton irradiation program at the northeast proton therapy center," in *Proc. IEEE IEEE Nuclear and Space Radiation Effects Workshop*, Monterey, CA, USA, Jul. 2003, pp. 141–144.

[11] H. H. K. Tang, "SEMM-2: A new generation of single event modeling tools," *IBM J. Res. Develop.*, vol. 52, no. 3, pp. 233–244, May 2008.

[12] H. H. K. Tang, G. R. Srinivasan, and N. Azziz, "Cascade statistical model for nucleon-induced reactions on light nuclei i the energy range of 50 MeV-1 GeV," *Phys. Rev.*, vol. C42, pp. 1598–1622, 1990.

[13] M. S. Gordon, P. Goldhagen, K. P. Rodbell, T. H. Zabel, H. H. K. Tang, J. M. Clem, and P. Bailey, "Measurement of the flux and energy spectrum of cosmic-ray neutrons on the ground," *IEEE Trans. Nucl. Sci.*, vol. 51, no. 6, pp. 3427–3434, Dec. 2004.

[14] SRIM: The Stopping and Range of Ions in Matter [Online]. Available: http://www.srim.org.

[15] E. Ibe, T. Toba, K. Shimbo, and H. Taniguchi, "Fault-Based reliable design-on-upper-bound of electronic systems for terrestrial radiation including muons, electrons, protons and low energy neutrons," in *Proc. 18th Int. On-Line Testing Symp.*, Sitges, Spain, Jun. 27-29, 2012, paper 3.2.

[16] J. F. Ziegler, "Terrestrial cosmic rays," *IBM J. Res. Develop.*, vol. 40, no. 1, pp. 19–39, Jan. 1996.

[17] E. Aguayo, A. S. Ankney, T. J. Berguson, R. T. Kouzes, J. L. Orrell, and M. D. Troy, "Cosmic ray interactions in shielding materials," Pacific Northwest National Lab., Richland, WA, USA, PNNL-20693, Tech. Rep., Jul. 2011.

[18] "Stopping powers for electrons and positrons," International Commission on Radiation Units and Measurements (ICRU) Rep. 37, Bethesda, MD, USA, Oct. 1, 1984.

[19] J. F. Ziegler, "Terrestrial cosmic ray intensities," *IBM J. Res. Develop.*, vol. 42, no. 1, pp. 117–139, Jan. 1998.

[20] M. Gordon, K. Rodbell, B. McNally, and S. Coleman, "Alpha counting, how long is enough?," in *Proc. IEEE Santa Clara Valley Soft Error Rate Workshop*, San Jose, CA, USA, Oct. 25, 2012 [Online]. Available: https://sites.google.com/site/ieeescvserworkshop/Presentations

[21] E. Yashchin, M. S. Gordon, and K. P. Rodbell, "Method of consumer producer raw material selection," patent pending, 2013.

[22] D. Cox and D. Hinkley, *Theoretical Statistics*. Boca Raton, FL, USA: Chapman & Hall, 1974.

[23] W. Rolke, A. Lopez, and J. Conrad, "Limits and confidence intervals in the presence of nuisance parameters," *Nucl. Instrum. Methods Phys. Res. A*, vol. 551, no. 2-3, pp. 493–504, Oct. 2005.